Sensors & Actuators: B. Chemical 350 (2022) 130873

Contents lists available at ScienceDirect

Sensors and Actuators: B. Chemical

journal homepage: www.elsevier.com/locate/snb

Broadband laser-based mid-infrared spectroscopy employing a quantum cascade detector for milk protein analysis

Alicja Dabrowska [a], Mauro David [b], Stephan Freitag [a], Aaron Maxwell Andrews [b], Gottfried Strasser [b], Borislav Hinkov [b], Andreas Schwaighofer [a,*], Bernhard Lendl [a,*]

[a] Institute of Chemical Technologies and Analytics, Technische Universität Wien, Getreidemarkt 9/164-UPA, 1060 Vienna, Austria
[b] Institute of Solid State Electronics & Center for Micro, and Nanostructures, Technische Universität Wien, Gußhausstrasse 25–25a, 1040 Vienna, Austria

ARTICLE INFO

Keywords:
Quantum cascade detector
Quantum cascade laser
Mid-infrared spectroscopy
Physical chemosensors
Milk protein analysis

ABSTRACT

Mid-infrared chemical sensors based on quantum cascade technology offer a number of properties surpassing conventional spectrometric techniques. In this work, we combine a tunable quantum cascade laser with a spectrally tailored in-house fabricated quantum cascade detector (QCD) to realize broadband detection of aqueous samples for selective sensing of bovine milk proteins. The developed setup enables broadband spectroscopy covering more than 260 cm^{-1} and was employed to record absorbance spectra of the amide I and amide II bands of β-lactoglobulin, α-lactalbumin and casein. A detailed comparison indicates similar performance of the laser-based setup with its uncooled QCD as a high-end FTIR spectrometer equipped with a liquid nitrogen cooled mercury-cadmium-telluride (MCT) detector. Furthermore, we discuss the characteristics and benefits of the quantum cascade detector for application in laser-based mid-infrared sensor systems and compare its performance to other common mid-infrared detector types. In conclusion, the combination of QCDs with EC-QCLs opens up new possibilities for next-generation MIR liquid-phase chemical sensors featuring low noise and high dynamic range.

1. Introduction

Mid-infrared (MIR) spectroscopy (4000 – 400 cm^{-1} / 2.5 – 25 μm) allows for highly selective, sensitive, and non-destructive sample investigation by probing molecular vibrations. IR spectroscopy techniques are widely used for quantitative and qualitative analysis in a variety of different fields, including the investigations of proteins [1,2]. Infrared spectra of proteins feature two characteristic absorption bands predominantly used for structural analysis. The amide I band (1600 – 1700 cm^{-1}) and amide II band (1500 – 1600 cm^{-1}) arise mainly from C═O stretching and N-H bending vibrations, respectively. The characteristic vibrations of these groups provide detailed information about the patterns of hydrogen bonding stabilizing secondary structures of proteins (i.e., α-helices, β-sheets, turns, and random structures) [1,2]. Thus, protein analysis by MIR spectroscopy plays an increasingly important role in medical, biochemical diagnostics, and food industry [2]. It is in particular an integrated part of the production workflow for quality assessment in the dairy industry [3]. Bovine milk contains ~32 g L^{-1} of proteins, 80% of which are caseins. The remaining 20% are whey proteins, among which the most abundant is β-lactoglobulin (~3.5 g L^{-1}) and α-lactalbumin (~1.2 g L^{-1}) [4]. For routine protein analysis, Fourier transform infrared (FTIR) spectroscopy incorporating thermal light sources (i.e. Globars) is considered the gold standard. However, employing this technique makes the analysis of protein samples usually a cumbersome task because of the strong water absorption band near 1645 cm^{-1}, overlapping with the amide I band and therefore significantly absorbing the radiation of a weak thermal light source (μW/cm^{-1}). This limits the applicable path lengths for transmission measurements to typically 5–8 μm, thus impairing the robustness of liquid sample handling and consequently complicating measurements of complex matrices such as milk [1]. Therefore, in commercial FTIR-based products, larger path length cells are in use (~35 μm), allowing protein analysis only in the amide II band region and thus limiting information on the protein secondary structure.

In this context, the significant advances of quantum cascade lasers (QCLs) [5] have challenged conventional MIR spectroscopy methods by offering much higher brightness (0.001 – 10 W/cm^{-1}) of MIR radiation, well suited for chemical sensing in highly absorbing solvents [6,7]. For

* Corresponding authors.
E-mail addresses: andreas.schwaighofer@tuwien.ac.at (A. Schwaighofer), bernhard.lendl@tuwien.ac.at (B. Lendl).

https://doi.org/10.1016/j.snb.2021.130873
Received 21 May 2021; Received in revised form 13 September 2021; Accepted 3 October 2021
Available online 7 October 2021

liquid-phase analysis, where molecules feature broad and complex absorption bands, commonly external cavity (EC-)QCLs are employed, providing tuning capabilities up to 500 cm^{-1} [8]. The power spectrum of EC-QCL sources is dictated by the gain material and thus fixed with characteristic highest intensities in the center and decreasing power towards both sides of the gain curve. Consequently, little to no flexibility exists to adjust the power levels of an EC-QCL across the tuning range. A number of studies employing EC-QCLs for broadband spectroscopy of liquids reported an improved detection over conventional FTIR spectroscopy for various analytes, including proteins [7,9,10]. High output powers of QCLs directly contributed to an almost fivefold increase in transmission path length [11], as required for robust sample handling and access to the amide I band thus enabling individual quantitation of bovine milk proteins in complex matrices [12–15], demonstrated monitoring of dynamic changes in the protein secondary structure [16–18], and showcased non-conventional ways for protein analysis exploiting the coherent nature of the QCL sources [19,20].

A detector optimized to the employed light source is another crucial part in a spectrometer or an optical sensor deciding on its final capabilities and performance. Nowadays, for MIR spectroscopy in classic FTIR spectrometers as well as in laser-based instruments, the two predominant types of employed detectors are either thermal or photonic [21]. The most common thermal detectors are based on the pyroelectric effect and consist of deuterated triglycine sulfate (DTGS). This type offers room-temperature operation, thus low maintenance, linear response, low price, but slow response times (kHz range), and is often employed for routine applications. The most widespread type of highly sensitive and fast MIR detectors and used in demanding applications are photonic detectors based on ternary semiconductor alloys made of mercury, cadmium and telluride, so called MCT detectors. They offer relatively fast response times (MHz range), broad responsivity regions and high sensitivity, but they require cooling to cryogenic temperatures by either liquid nitrogen or thermoelectric cooling to cut thermal noise. A downside of these otherwise powerful detectors is their rather limited dynamic range, which is of special relevance when mid-IR radiation of strongly varying intensities need to be detected and processed. This is the case when employing EC-QCLs for measurements of aqueous solutions in a spectral range that includes the strong bending vibration of water centered at 1645 cm^{-1}. In such a situation the water background will strongly limit throughput, dictating the use of a short pathlength. On the contrary, the short path lengths result in high intensities in neighboring regions. In order to stay within the limited dynamic range of the previously mentioned detectors during a full spectral scan of the employed EC-QCL, additional optical components had to be incorporated in laser-based spectrometers dedicated for protein analysis to attenuate the laser beam before impinging the detector to avoid its saturation [9,22]. These actions negate the high-power advantage of QCLs, complicate the setup, and reduce its versatility and range of applications.

In this context, accompanied by the developments in QCLs, there has been also progress in quantum engineering-based detectors, which offer properties much better suited to combine with QCLs, allowing to evoke the full potential of these sources for challenging spectroscopic applications.

Quantum cascade detectors (QCDs) [23] are intersubband photodetectors operated in the zero-bias (photovoltaic) or low bias mode by design, enabling fast detection (GHz regime) at room temperature, limited only by the thermal Johnson-Nyquist noise [24–27]. Analogous to QCLs, QCDs use the same materials (typically InGaAs/InAlAs/InP), design, and fabrication processes (e.g. molecular beam epitaxy, MBE). So far, applications of QCDs for spectroscopic detection in the MIR are predominantly focused on gas-phase analysis. Here, monolithic integration for miniaturized gas-sensing devices was demonstrated [6, 28–32]. For liquid-phase analysis, the reports are limited to single wavelength detection in conjunction with distributed feedback QCLs as light sources [31]. A single attempt toward the use of QCDs for wideband detection was reported using a spectrally broad QCD in combination with a Globar to characterize the transmission of a sapphire wafer [33].

An advantage of QCDs particularly profitable for laser-based spectroscopy of liquids is the detection across a wide power range of the incident radiation without saturation effects [34]. This high dynamic range is beneficial when broadband, high-power QCLs are employed for measuring spectra covering regions with high intensity (low solvent absorption) and low intensity (high solvent absorption), as is the case for IR protein analysis in aqueous solutions. Hence, no attenuating optical components are needed to remain in the linear regime of the detector as is necessary when using MCT detectors.

In this work, we combine a widely tunable EC-QCL with a spectrally tailored in-house developed QCD to record broadband infrared spectra of synthetic milk protein samples to demonstrate the possibilities for laser-based transmission spectroscopy presented by the combination of these two components. To our best knowledge, this is the first report on the use of a QCD in an EC-QCL-based system for broadband investigation of a liquid media in such a wide spectral range (>260 cm^{-1}). First, we demonstrate the characteristics of the developed QCD and compare them to established MIR detector types. Next, we present broadband IR transmission spectra of bovine milk proteins, i.e. casein, β-lactoglobulin and α-lactoglobulin recorded by the novel EC-QCL-QCD setup and conduct qualitative and quantitative analysis. We compare the performance of the custom-made sensor system to FTIR spectroscopy. Moreover, to exploit the benefits of the large available spectral region and to show a more practical application, we apply chemometric tools to investigate ternary milk protein mixtures.

2. Experimental section

2.1. Experimental setup for broadband QCL-based IR spectroscopy using QCD

A schematic of the experimental setup for broadband absorption spectroscopy of liquid-phase samples employing an EC-QCL and a QCD is depicted in Fig. 1. In principle, the setup measures the attenuation of light transmitted through a liquid sample at different frequencies (wavenumbers) induced by absorption to identify and quantify proteins present in the sample. For this purpose, a thermoelectrically (TE) cooled external-cavity quantum cascade laser (Hedgehog, Daylight Solutions Inc., San Diego, CA), tunable from 1830 to 1470 cm^{-1}, was operated in pulsed mode at a modulation frequency of 1 MHz, duty cycle of 20% and a laser current of 700 mA, corresponding to a pulsed average power of

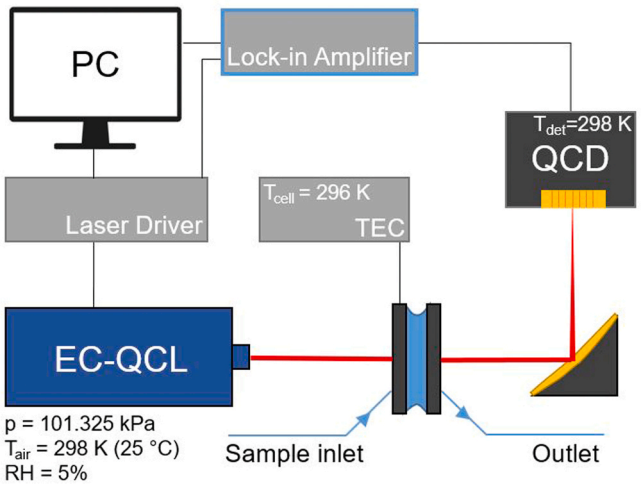

Fig. 1. Experimental setup employing an EC-QCL and a ridge QCD for broadband sensing of bovine milk proteins in transmission configuration.

approx. 240 mW at 1590 cm^{-1}. The laser operation parameters were selected to maximize optical power output and the amount of light available for the light-sample interaction and hence the applicable path length for transmission measurements. The p-polarized laser beam was directed into a custom-made temperature-stabilized (23.0 °C, 296 K) by a thermoelectrical cooler (TEC, Meerstetter Engineering) transmission flow cell with a 12.5 μm PTFE spacer between 25 × 15 × 1 mm thick CaF_2 wedged windows. The transmission path length was optimized to achieve the highest signal-to-noise (SNR) ratio for protein measurements in the presented system (Fig. S1). The transmitted beam was focused by a parabolic gold mirror (Thorlabs MPD229M01) on the facet of the QCD and butt-coupled to its active region. The detector chip (15 × 25 mm) with an integrated printed circuit board (PCB, top contact) was attached to a copper plate (bottom contact). The QCD was operated at room temperature (298 K). The detector signal output (photovoltage) was connected via a coaxial cable directly to a low-noise voltage input of a MFLI lock-in amplifier (MFLI, Zurich Instruments AG, Zurich, Switzerland) to measure the detector response at the reference frequency corresponding to the laser modulation frequency supplied by a laser driver via a TTL signal and thus improve the SNR of the whole detection scheme. The lock-in amplifier was equipped with an extended cut-off range of 5 MHz. The experimental setup was operated at ambient conditions (pressure of 101.325 kPa, temperature of 298 K) at low relative humidity (RH) level of ~5%. The optical setup was housed and purged with dry air prior and during measurements to minimize adverse effects of water vapor bands in the investigated spectral region.

2.2. QCD device

The QCD used in the experimental setup was designed, grown, and processed in-house. The device is based on an $In_{0.53}Ga_{0.47}As/Al_{0.48}In_{0.52}As$ active region (AR), grown lattice matched on a low-doped InP substrate (n~$1 \cdot 10^{17}$ cm^{-3}) by molecular beam epitaxy (MBE) in our in-house cleanroom facilities. It is optimized for detection around 6.5 μm wavelength, targeting the spectral region of the previously mentioned two most prominent absorption bands of proteins (amide I and amide II).

Similar to QCLs, the target wavelength is achieved by careful balancing the optical intersubband transition through so-called band-structure engineering of the highly complex quantum structure. This means, that the sequence of quantum wells in the AR is modified by changing their geometry (i.e., the thickness of mainly the InGaAs wells and to a lesser extent the AlInAs barriers) in such a way, that the energy separation between upper and lower lasing level in the quantum wells corresponds to the wanted wavelength. This enables addressing various wavelengths throughout the MIR spectral range by simply changing the geometry of the AR [5], while still using the very same material system.

To increase the spectral overlap with the absorbed photons, in total 35 periods of the InGaAs/InAlAs AR sequence (each 75.5 nm thick, total AR thickness: 2.64 μm) are implemented in our design. They are sandwiched between two $In_{0.53}Ga_{0.47}As$ separate confinement layers (doped: n~$5 \cdot 10^{16}$ cm^{-3}, thickness: 550 nm (bottom) and 400 nm (top)). On top of this structure, the upper cladding is grown, consisting of ~2 μm of $Al_{0.48}In_{0.52}As$ followed by 360 nm of $In_{0.53}Ga_{0.47}As$. To mitigate the negative effects of free carrier absorption in the MIR [35], while still allowing good ohmic contacts, the doping is gradually increased throughout the cladding layer starting at a low value of n~$1 \cdot 10^{17}$ cm^{-3} close to the AR and ending at n~$1 \cdot 10^{20}$ cm^{-3} for the last 10 nm of the top-most InGaAs contact layer. More details on the active region design can be found elsewhere [6,34].

In contrast to previous publications of this active region design, where MESA-type of geometries for out-off-plane outcoupling through the sample surface were used (e.g. [6,34]), the QCDs for the experiments in this paper were fabricated into ridge waveguides (see Fig. 2). This configuration was selected for several reasons: first of all, it best matches the outcoupled mode-profile from the used EC-QCL, which, together with the relatively wide facets of 10 – 20 μm, allows the most efficient free-space coupling of the QCL beam to the QCD, by using a standard parabolic gold mirror (see experimental setup in Fig. 1) and simply butt-coupling the light perpendicular to the QCD facet. Second, directing the light perpendicular to the growth direction of the device allows direct coupling of the light, without the need for complex grating coupling structures, as needed for surface coupling to adapt for the TM polarization of the transition (originating from the quantum mechanical selection rules of intersubband transitions) [36]. And third, in future developments it allows to directly integrate the whole setup into a monolithic geometry with laser, interaction section and detector on the same chip, as shown in a proof-of-concept study [31], using a similar ridge geometry as we do in this work.

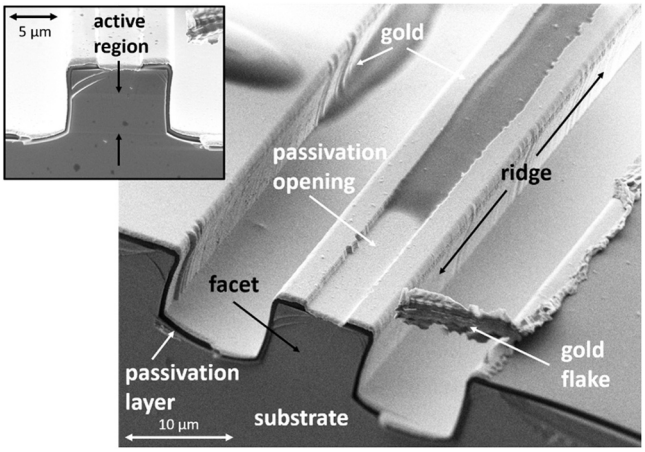

Fig. 2. Scanning Electron Microscope (SEM) image of a typical 10 μm ridge waveguide QCD used in this study. The opening in the center on top of the ridge in the passivation layer can be identified as well as the "shiny" metallization layer covering the whole device. The thin black passivation layer prevents the electrical current from by-passing the active region and directly flowing into the (dark grey) substrate. (Inset): View on the front facet of a 10 μm ridge waveguide. The InGaAs/InAlAs active region can be identified as slightly lighter layer on the front facet as compared to the surrounding InP top cladding (above) and substrate (below).

2.3. Data acquisition and processing

Broadband absorbance spectra of proteins in aqueous solution were recorded in the spectral region between 1470 and 1730 cm^{-1} allowing to investigate the full span of the amide I and amide II bands. A spectrum was acquired by continuous tuning of the grating of the EC-QCL selecting subsequent emission wavenumbers across the spectral range with a tuning speed of 3600 cm^{-1} s^{-1} and a spectral resolution of 0.4 cm^{-1} enabled by the small laser linewidth (<0.5 cm^{-1} at FWHM). The varying intensity across the tuning range was recorded by the QCD. Three hundred scans were averaged per spectrum, with a total acquisition time of 45 s. A small fraction (1–3%) of scans deviating from the rest due to acquisition errors were eliminated with a similarity index below 0.84 [22]. The spectra were wavenumber-calibrated using the absorption bands of water vapor to reduce wavenumber deviations caused by inaccuracies introduced by the EC-QCL and delays in data acquisition [11]. The recorded IR spectra were filtered using a fast Fourier transform (FFT) filter with a cut-off frequency of 1500 Hz, yielding a spectral resolution of 2.6 cm^{-1}. The absorbance spectra were derived by calculating the negative decadic logarithm of the sample signal I_S divided by the solvent signal I_{BG}, $A = -\log_{10}(I_s/I_{BG})$. Data acquisition was performed using an in-house developed Python script (Python 3.7) to access the MFLI API. Data processing was performed with an in-house developed MATLAB 2020a script and spectral evaluation was conducted in OPUS 8.1 (Bruker Corp., Ettlingen, Germany).

2.4. Reference FTIR measurements

FTIR absorption spectra were recorded on a Vertex 80v FTIR spectrometer (Bruker Corp., Ettlingen, Germany) equipped with a Globar (MIR source, 12 V, dedicated to Vertex 80v FTIR spectrometer, Bruker Corp., Ettlingen, Germany) and a liquid nitrogen (LN_2) cooled MCT detector ($D^* = 4.0 \cdot 10^{10}$ cm $Hz^{1/2}$/W at 9.2 μm) and a Bruker Tensor 37 FTIR spectrometer equipped with a DLaTGS detector ($D^* = 6.0 \cdot 10^8$ cm $Hz^{1/2}$/W at 9.2 μm). Samples were measured at 25 °C in a transmission cell equipped with two 2-mm-thick CaF_2 windows and an 8 μm PTFE spacer. A total of 262 (Vertex 80v, scanner speed 80 kHz) and 36 (Tensor 37, scanner speed 10 kHz) scans were averaged per spectrum, corresponding to an overall acquisition time of ~45 s. Spectra were recorded with a resolution of 2.6 cm^{-1} and were calculated using a Blackman-Harris 3-term apodization function and zero filling factor of 2. The sample compartment of the FTIR instruments was purged with dry air prior to and during spectrum acquisition and in case of using the Vertex 80v FTIR spectrometer the remaining part of the spectrometer was also evacuated (2.88 hPa). Spectra were analyzed with the OPUS 8.1 software package (Bruker Corp., Ettlingen, Germany).

2.5. Reagents and samples

Lyophilized powders of casein sodium salt (Cas, ≥70%), α-lactalbumin (α-LA, ≥85%) and β-lactoglobulin (β-LG, ≥85%) from bovine milk were purchased from Sigma-Aldrich (Steinheim, Germany). Individual stock solutions of respective proteins were prepared in 16 mmol L^{-1} sodium phosphate buffer (pH 7.5; + 0.1 M NaCl) and diluted to eight concentrations ranging from 0.25 to 15 mg mL^{-1}. For multivariate analysis, a calibration sample set consisting of 15 samples of ternary protein mixtures (α-LA, β-LG, Cas) was prepared and diluted in a buffer, reaching concentrations of individual and total protein of 1–10 mg mL^{-1} and 5.5–21 mg mL^{-1}, respectively. Ultrapure water (18 MΩ) from a Milli-Q water purification system (Millipore, Bedford, USA) was used for the preparation of all solutions.

3. Results and discussion

3.1. QCD characterization and parameter comparison

After fabrication, the QCD device was characterized. The broadband ridge detector photo-signal spectrum was measured at room temperature with a Globar [34]. Spectral FTIR characterization revealed a wide usable spectral range of the detector response spanning 1100–2100 cm^{-1} (threshold defined at 15% of the maximum signal value) (Fig. S2). Hence, the emission profile of the used EC-QCL (1470 cm^{-1} – 1830 cm^{-1}) stays within the given detection range of the QCD (Fig. 3A). The room-temperature spectral responsivity R(λ) was measured using the EC-QCL (Eq. (1)). The peak responsivity R_P was found to be 143 mA/W at 1540 cm^{-1} (6.49 μm), without additional amplification (Fig. 3B):

$$R(\lambda) = \frac{I_{ph}}{P_i} \quad \left[\frac{A}{W}\right], \tag{1}$$

where P_i is the incident radiation power and I_{ph} the photocurrent. For the calculation, the laser power was normalized to the ridge geometry, as only the light entering through the ridge facet is coupled to the QCD. The specific detectivity D^* measured at room temperature (298 K) is 2.44×10^6 cm$\sqrt{(Hz)}$/W:

$$D^* = \frac{R_P}{i_n}\sqrt{A\Delta f} \quad \left[\frac{cm\sqrt{Hz}}{W}\right], \tag{2}$$

where i_n is the root mean square noise current, A is detector area and Δf is the measurement bandwidth.

The parameters of the employed detector significantly influence the performance of the overall sensor system. To put the advantages of the newly introduced QCD into perspective, its parameters were compared to other detector types, which are routinely combined with EC-QCLs for MIR spectroscopy, namely TE-cooled MCTs and pyroelectric detectors [9–16,19,20]. An overview of the most important features and properties of these detector types are summarized in Table 1.

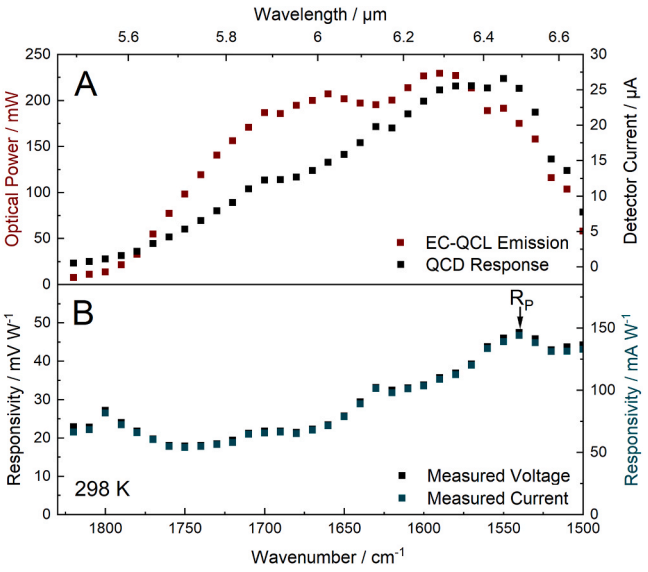

Fig. 3. (A) EC-QCL emission spectrum (left scale) and QCD photocurrent spectrum (right scale). (B) QCD spectral responsivity measured at room temperature with an EC-QCL.

To assess the linearity and response characteristics of the discussed detectors (Fig. 4), their response was measured at 1590 cm^{-1} in pulsed mode (modulation frequency: 1 MHz, pulse width 200 ns) for QCD and TE-cooled MCT detector (PVI-4TE-10.6, Vigo S.A, Poland). The pyrodetector response was measured in CW laser mode with a mechanical chopper providing 40 Hz modulation frequency with a time constant of 61 ms. A mesh was used to attenuate the laser beam to avoid pyroelectric detector saturation.

Even though they are not directly in this comparison, a further kind of IR detectors that should be mentioned are the LN_2-cooled MCTs. They are typically employed for high-end FTIR spectroscopy in laboratory settings. Liquid nitrogen provides cooling down to 80 K, which is needed to provide low noise levels at the low light intensities emitted by thermal light sources. However, the dewars holding the coolant are bulky and require frequent refilling. These parameters prevent miniaturization and

Table 1
Characteristics of detectors for laser-based IR spectrometers.

	QCD	TE-cooled MCT	Pyroelectric
Device active area[a]	2.64 × 10 μm^2	1 × 1 mm^2	2 × 2 mm^2
Cooling / Operation temperature	optional[b] / room temp.	yes / 202 K	no / room temp.
Speed / Cut-off frequency range	DC - GHz regime	DC - MHz regime	DC - Hz regime
Spectral range	NIR - THz	MIR	UV - THz
Spectral range of a single unit	narrow (matched to QCL)	medium (few μm)	broad
Linearity	high	poor	high
Saturation threshold	very high	low (few mW)	low (few mW)
Noise density[a] [μV/√Hz]	0.001	0.75	57
Detectivity[a] [cm√Hz/W]	2.44•10^6	9.2•10^8	4.00•10^8

[a] values stated for particular detector units used for comparison;
[b] cooling can be applied to achieve higher detectivity.

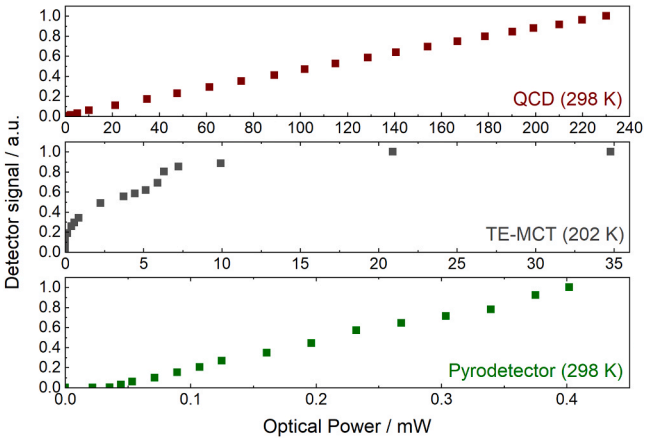

Fig. 4. Comparison of the dynamic response of the 3 compared MIR detectors.

applications as envisioned for laser-based sensor systems.

In contrast, TE-cooled MCTs feature greater compactness and typically provide cooling to 202 K which is required for increased detectivity. They were successfully used for many laser-based applications due to their high sensitivity, bandwidth (MHz regime), flexibility, and broad spectral detection range (few μm). Their bandwidth allows to record spectra at high pulse frequencies, which also enables measurement at high laser sweeping rates [37]. However, their well-known flaws are a nonlinear response and low saturation thresholds, as shown in Fig. 4. Consequently, reliable quantitative measurements require careful consideration and optimization of the light intensities at the detector across the measured spectral region. Strongly absorbing solvents such as water lead to uneven spectral power densities across the protein amide I and II region and thus require the introduction of carefully selected intensity filters [9,22]. This approach consequently limits the use only to a strictly defined application (i.e., solvent system), thus affecting the versatility of the instrument. Furthermore, these additional optical elements often introduce disruptive fringes into the system negatively affecting the detected signal [9].

Pyroelectric detectors, although less popular than MCTs, have also been used in combination with EC-QCLs for sensing in liquids [20]. This technology is characterized by a high-linearity, modest-sensitivity, room-temperature operation, small sizes, and a broad spectral response (i.e., homogeneous absorption of radiation from UV to THz). Due to the slow response times (milliseconds), this detector type is usually employed to record laser-based spectra in the step-and-measure mode [7,20].

In turn, QCDs maintain excellent linearity for much higher radiation power than the other two detector types, as depicted in Fig. 4. This means that the full extent of QCL beam intensity is available for spectroscopy with a linear response that allows for quantitative analysis. In addition to the high saturation threshold, QCDs also offer high sensitivity at low intensities in case of cooling to cryogenic temperatures, which can enable path length extensions for measurements in transmission. Employing the room-temperature operated QCD, as presented in this study, optical path lengths up to 18.5 μm could be used for protein measurements in transmission within the given concentration range, without a significant increase in noise caused by the signal loss. However, the highest SNR was achieved at the optical path length of 12.5 μm and hence this length was selected for further measurements with the presented system (see Fig. S1 in Appendix A). The achievable noise level is theoretically only limited by Johnson-Nyquist noise, mainly due to its unbiased operating conditions. Consequently, a wide dynamic range is applicable. No additional optical components, e.g., filters, need to be employed for spectroscopically complex solvent-analyte combinations, thus increasing the setup's simplicity and versatility and reducing its costs.

3.2. Broadband MIR spectra of proteins recorded with the EC-QCL-QCD setup

An experimental EC-QCL-QCD sensor system was used to record MIR spectra of the most abundant bovine milk proteins featuring different secondary structures at varying concentrations. Broadband tuning capabilities of the employed EC-QCL combined with a spectrally matched QCD allowed to record the full spectral range covering the amide I and amide II bands. Fig. 5A–C presents the acquired absorbance spectra of β-LG, α-LA and Cas. β-LG is mainly composed of β-sheet secondary structure which gives rise to a broad amide I band maximum at ~1632 cm^{-1} with a sideband at 1680 cm^{-1} and an amide II band with a maximum at 1550 cm^{-1} [38]. α-LA predominantly composed of α-helical structures shows a distinct amide I band maximum at 1653 cm^{-1} and an amide II band maximum at 1550 cm^{-1} [39]. Casein features an irregular α-helix and β-sheet structure, which results in band maxima at 1651 cm^{-1} and 1550 cm^{-1} in the amide I and amide II bands, respectively [40,41]. Furthermore, EC-QCL-QCD spectra were compared with FTIR absorbance spectra (Fig. 5D–F). Evaluation of the band shape and peak position corresponding to secondary structures show an excellent agreement between the custom-made (EC-QCL-QCD) sensor system and the reference instrument (FTIR). In this regard, the degree of spectral overlap (s_{12}) was calculated between EC-QCL-QCD (s_1) and FTIR spectra (s_2) and it was found to be > 0.997 (see Appendix A) [42]. Small artifacts on EC-QCL-QCD spectra were due to the presence of residual water vapor in the experimental system. Quantitative evaluation of the height of the band maxima in the amide I region was performed. Calibration curves (Fig. S3) show high linearity (R^2 >0.998) in the measured concentration range from 15 mg mL^{-1} down to 0.25 mg mL^{-1}. The obtained results show the good performance of the custom-made setup for qualitative as well as quantitative protein analysis.

3.3. Performance comparison of the EC-QCL-QCD setup to FTIR spectroscopy

The EC-QCL-QCD sensor system was benchmarked against a routine FTIR instrument using a Globar equipped with a pyroelectric (DLaTGS) detector operated at room temperature and a high-end FTIR instrument with a LN_2-cooled MCT detector. For noise level evaluation, 100% transmission lines were recorded at similar acquisition times (~45 s) and spectral resolution (2.6 cm^{-1}) by every instrument. The root-mean-square (RMS) noise of the 100% lines of water was calculated in the spectral region between 1700 and 1600 cm^{-1}. Furthermore, the limit of detection (LOD) was assessed by taking into account the RMS noise level and the slope of the calibration curve of individual proteins, as follows:

$$LOD = \frac{3 \bullet noise_{RMS}}{slope \quad of \quad the \quad calibration \quad curve}. \tag{3}$$

Characteristic instrument parameters and the results of the comparison are in Table 2. With the noise level of 6.7×10^{-5} AU achieved by the EC-QCL-QCD setup, the LODs of 0.088, 0.079, 0.095 mg mL^{-1} were determined for β-LG, α-LA and Cas, respectively. When comparing the laser-based-QCD setup with the routine FTIR spectrometer operated at room temperature, an LOD and noise better by a factor of 5–6 was accomplished. Here, a contributing factor to the lower noise level of the EC-QCL-QCD setup is the higher number of scans in the same time period enabled by the high laser sweep rate (i.e., 3600 cm^{-1}/s).

The noise level and LOD achieved by EC-QCL-QCD setup best compares to high-end FTIR spectrometer. Here, the noise levels and LODs are within the same range, indicating excellent performance of the custom-made sensor system and ensuring its capability for high-quality measurements. Even though the detectivity of the employed QCD is much lower (~16 000 times) than the one of the LN_2-cooled MCT, its combination with the high-power laser (~10^4 higher W/cm^{-1} than Globar) leads to comparable performance of the EC-QCL-QCD setup to the high-end FTIR spectrometer. The combination of EC-QCL with uncooled QCD

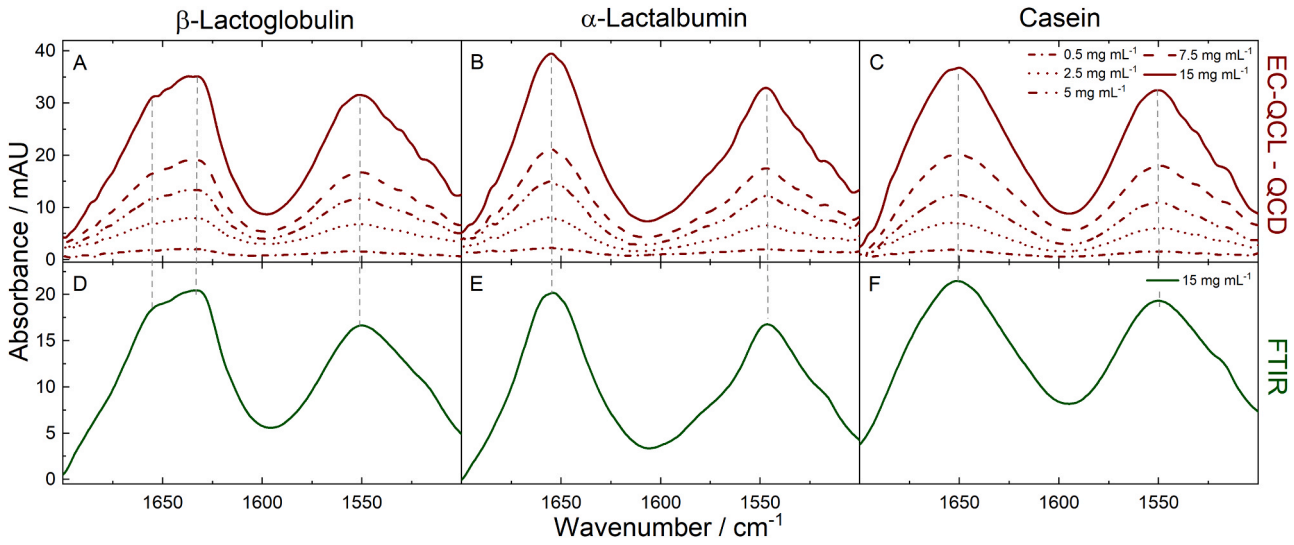

Fig. 5. (A-C) MIR absorbance spectra of bovine milk proteins with concentrations of 0.5, 2.5, 5, 7.5 and 15 mg mL^{-1} acquired by the EC-QCL-QCD based setup. (D-F) Reference FTIR absorbance spectra of 15 mg mL^{-1} bovine milk proteins recorded by a high-end FTIR instrument. Vertical gray dashed lines indicate an excellent overlap of spectral features (i.e. peak positions) between the MIR spectra acquired by laser-based setup and FTIR instrument.

Table 2
Comparison of EC-QCL and QCD-based setup with conventional FTIR spectroscopy.

	Detector / Temp. / Cooling	RMS-Noise 10^{-5} / AU	LOD[a] / g L^{-1}	Path length / μm	Measuring time / scans	Spectral range
EC-QCL - QCD	ridge QCD / 298 K / —	6.7	0.088	12.5	45 / 300	1700–1500
Routine FTIR	DLaTGS / 298 K / —	26.7	0.494	8	45 / 36	4000–1000
High-end FTIR	MCT / 80 K / LN_2	2.3	0.041	8	45 / 262	4000–1000

[a] Defined for β-LG.

also allowed to extend the optimum transmission path length for the experiment, thus improving the robustness of liquid handling and facilitating the analysis of samples with complex matrix. This is due to the fact that the pressure drop encountered in the cell inversely scales with the third power of the used path length (assuming constant, laminar flow through a flat rectangular channel) and even small extension in path length lead to significant reduction of the encountered pressure drop in the cell [43]. In this context, it must be noted that the detectivity of a QCD can be easily increased up to several orders of magnitude by device cooling [24,33,34], leaving much room for future improvements.

The spectral accessibility was also compared. In contrast to the more versatile and broadband FTIR instruments, the accessible region of the QCL-QCD device is restricted not only by the emission gain of the laser but also the detector's spectral coverage. Therefore, these two components need to be matched so that their emission and detection profiles overlap to target specific areas of application.

3.4. Multivariate quantification of milk protein mixtures

In order to test the capabilities of the developed setup for quantification of complex analyte mixtures, multivariate quantitation of ternary milk protein samples was performed using partial least squares (PLS) regression models (multiple PLS1 models). PLS is a multivariate statistical approach capable of calculating linear regression models from highly correlated variables usually found in spectroscopic data. Hence, the algorithm is routinely used for simultaneous quantitation of multiple proteins based on their MIR absorption spectra [13,15,44]. Spectral decomposition is performed by the evaluation of spectral profiles in the wavenumber regions featuring the highest specificity for individual proteins. Although, theoretically, chemometric analysis can be applied to very narrow, single-point regions, collective analysis of broader spectral regions, i.e. both amide I + II bands, can provide more robust and accurate prediction models for selective protein quantitation [45,46]. In this context, 15 synthetic solutions containing ternary mixtures of bovine milk proteins at relevant concentrations were prepared as calibration set. The corresponding spectra recorded by the EC-QCL-QCD setup (Fig. S4) were evaluated by PLS modelling (PLS Toolbox 8.8.1, Eigenvectors Research Inc). Detailed information about the nominal and predicted milk protein concentrations for a calibration set is given in Table S1 and Fig. S5 (see Appendix A). Table 3 summarizes the PLS parameters and calibration results for each model. Spectral ranges for the analysis were restricted based on the selectivity ratio [47,48]. Spectra were preprocessed using mean centering and derivative transformation. The optimal number of latent variables was determined by leave-one-out cross validation. As shown in Table 3, the obtained figures of merit show high coefficients of determination (R^2) of calibration (>0.98) and satisfactory root-mean-square errors of calibration (RMSEC) and cross-validation (RMSECV), indicating very good model

Table 3
PLS calibration parameters and internal figures of merit.

	β-LG	α-LA	Cas	Total protein
Concentration range / mg mL^{-1}	1.0–10.0	1.0-10.0	1.0-10.0	5.5–21.0
Spectral region / cm^{-1}	1597–1652	1547–1654	1505–1720	1520–1561
Preprocessing	MC, 1st Der	MC, 1st Der	MC, 1st Der	MC
LVs	3	3	4	2
Exp. Var. / %	99.20	99.30	99.24	98.12
RMSEC / mg mL^{-1}	0.226	0.220	0.231	0.653
RMSECV / mg mL^{-1}	0.309	0.302	0.426	0.765
R^2 Cal	0.992	0.993	0.992	0.981
R^2 CV	0.985	0.987	0.976	0.974

MC: mean centering; 1st Der: first derivative calculated using Savitzky-Golay filter (order: 2, window 15 points/0.5 cm^{-1}); LVs: latent variable(s); RMSEC: root-mean-square error of calibration; RMSECV: root-mean-square error of cross-validation; R^2: coefficient of determination; Cal: calibration; CV: cross-validation.

performance. The overall results showcase the ability of the EC-QCL-QCD setup to adequately quantify complex protein mixtures with different secondary structures.

4. Conclusion and outlook

In this study, we demonstrated the first use of a QCD in combination with an EC-QCL for broadband MIR spectroscopy of liquid-phase samples. We presented the successful application of this detector type operated at room temperature for detection and analysis of synthetic milk protein samples by recording broadband absorbance spectra of the amide I and amide II bands in transmission. We further demonstrated that our EC-QCL-QCD sensor system has equal performance for protein analysis as high-end FTIR spectroscopy, while maintaining much greater compactness and simplicity.

The QCD technology, although developed over 20 years, is still in its infancy in the field of spectrometric applications, particularly for detection in liquid phase. We showcased that a detection band of a QCD is wide enough to be paired with a broadly tunable EC-QCL in a free-space setup that performs well enough to study complex analytical problems. In this context, it was found that QCDs can be considered as a well-performing and reliable detector unit compared to TE- or LN_2-cooled MCTs, and pyroelectric detectors, used in broadband laser-based spectrometers. They offer the advantage of room-temperature operation, low power consumption, excellent linearity, low noise, high bandwidth, high speed, and high saturation thresholds. In conclusion, QCDs paired with EC-QCLs can be considered as well-matched building blocks for the next-generation MIR liquid-phase chemical sensors delivering high-quality information within broader spectral ranges. Their high potential for integration ensured by ongoing progress in semiconductor technology paves the way for the development of miniaturized and portable sensors in on-chip configurations.

CRediT authorship contribution statement

Alicja Dabrowska: Conceptualization, Investigation, Formal Analysis, Visualization, Writing – original draft. **Mauro David:** Resources, Investigation. **Stephan Freitag:** Conceptualization, Writing – review & editing. **Aaron Maxwell Andrews:** Resources, Writing – review & editing. **Gottfried Strasser:** Resources, Funding acquisition, **Borislav Hinkov:** Resources, Writing – review & editing. **Andreas Schwaighofer:** Supervision, Funding acquisition, Writing – review & editing. **Bernhard Lendl:** Conceptualization, Supervision, Resources, Funding acquisition.

Declaration of Competing Interest

The authors declare that they have no known competing financial interests or personal relationships that could have appeared to influence the work reported in this paper.

Acknowledgments

This work has received funding from the European Union's Horizon 2020 research and innovation program under grant agreement no. 780240 as well as from the COMET Center CHASE (project No 868615), which is funded within the framework of COMET (Competence Centers for Excellent Technologies) by BMVIT, BMDW, and the Federal Provinces of Upper Austria and Vienna. The COMET program is run by the Austrian Research Promotion Agency (FFG). A.S. acknowledges funding by the Austrian Science Fund FWF (P32644-N). A.M.A acknowledges funding by the AFOSR-EOARD (FA9550–17-1–0340).

Appendix A. Supporting information

Supplementary data associated with this article can be found in the online version at doi:10.1016/j.snb.2021.130873.

References

[1] H. Fabian, W. Mäntele, Infrared Spectroscopy of Proteins, in: J.M. Chalmers (Ed.), Handb. Vib. Spectrosc., John Wiley & Sons, Ltd, Chichester, UK, 2006. ⟨http://doi.wiley.com/10.1002/0470027320.s8201⟩ (accessed March 24, 2020).
[2] A. Barth, Infrared spectroscopy of proteins, Biochim. Biophys. Acta - Bioenerg. 1767 (2007) 1073–1101, https://doi.org/10.1016/j.bbabio.2007.06.004.
[3] A. Kohler, N.K. Afseth, K. Jørgensen, Å. Randby, H. Martens, Quality Analysis of Milk by Vibrational Spectroscopy, in: E.C.Y. Li-Chan (Ed.), Handb. Vib. Spectrosc., John Wiley & Sons, Ltd, Chichester, UK, 2010, https://doi.org/10.1002/0470027320.s8957.
[4] P.F. Fox, T. Uniacke-Lowe, P.L.H. McSweeney, J.A. O'Mahony, Milk Proteins, in: Dairy Chem. Biochem., Springer International Publishing, Cham, 2015, pp. 145–239, https://doi.org/10.1007/978-3-319-14892-2_4.
[5] J. Faist, F. Capasso, D. Sivco, C. Sirtori, A. Hutchinson, A. Cho, Quantum cascade laser, Science (80-.) 264 (1994) 553–556, https://doi.org/10.1126/science.264.5158.553 (ARTICLE).
[6] A. Harrer, R. Szedlak, B. Schwarz, H. Moser, T. Zederbauer, D. MacFarland, H. Detz, A.M. Andrews, W. Schrenk, B. Lendl, G. Strasser, Mid-infrared surface transmitting and detecting quantum cascade device for gas-sensing, Sci. Rep. 6 (2016) 21795, https://doi.org/10.1038/srep21795.
[7] A. Schwaighofer, B. Lendl, Quantum Cascade Laser-based Infrared Transmission Spectroscopy Of Proteins In Solution, in: Vib. Spectrosc. Protein Res., Elsevier, 2020, pp. 59–88.
[8] S. Riedi, A. Hugi, A. Bismuto, M. Beck, J. Faist, Broadband external cavity tuning in the 3-4 μ m window, Appl. Phys. Lett. 103 (2013), 031108, https://doi.org/10.1063/1.4813851.
[9] C.K. Akhgar, G. Ramer, M. Żbik, A. Trajnerowicz, J. Pawluczyk, A. Schwaighofer, B. Lendl, The next generation of IR spectroscopy: EC-QCL based mid-IR transmission spectroscopy of proteins with balanced detection, Anal. Chem. 92 (2020) 9901–9907, https://doi.org/10.1021/acs.analchem.0c01406.
[10] A. Schwaighofer, C.K. Akhgar, B. Lendl, Broadband laser-based mid-IR spectroscopy for analysis of proteins and monitoring of enzyme activity, Spectrochim. Acta Part A Mol. Biomol. Spectrosc. 253 (2021), 119563, https://doi.org/10.1016/j.saa.2021.119563.
[11] M.R. Alcaráz, A. Schwaighofer, C. Kristament, G. Ramer, M. Brandstetter, H. Goicoechea, B. Lendl, External-cavity quantum cascade laser spectroscopy for mid-ir transmission measurements of proteins in aqueous solution, Anal. Chem. 87 (2015) 6980–6987, https://doi.org/10.1021/acs.analchem.5b01738.
[12] J. Kuligowski, A. Schwaighofer, M.R. Alcaráz, G. Quintás, H. Mayer, M. Vento, B. Lendl, External cavity-quantum cascade laser (EC-QCL) spectroscopy for protein analysis in bovine milk, Anal. Chim. Acta 963 (2017) 99–105, https://doi.org/10.1016/j.aca.2017.02.003.
[13] A. Schwaighofer, J. Kuligowski, G. Quintás, H.K. Mayer, B. Lendl, Fast quantification of bovine milk proteins employing external cavity-quantum cascade laser spectroscopy, Food Chem. 252 (2018) 22–27, https://doi.org/10.1016/j.foodchem.2018.01.082.
[14] A. Schwaighofer, M.R. Alcaráz, J. Kuligowski, B. Lendl, Recent advancements of EC-QCL based mid-IR transmission spectroscopy of proteins and application to analysis of bovine milk, Biomed. Spectrosc. Imaging 7 (2018) 35–45, https://doi.org/10.3233/bsi-180177.
[15] M. Montemurro, A. Schwaighofer, A. Schmidt, M.J. Culzoni, H.K. Mayer, B. Lendl, High-throughput quantitation of bovine milk proteins and discrimination of commercial milk types by external cavity-quantum cascade laser spectroscopy and chemometrics, Analyst 144 (2019) 5571–5579, https://doi.org/10.1039/c9an00746f.
[16] A. Schwaighofer, M.R. Alcaraz, L. Lux, B. Lendl, pH titration of β-lactoglobulin monitored by laser-based Mid-IR transmission spectroscopy coupled to chemometric analysis, Spectrochim. Acta - Part A Mol. Biomol. Spectrosc. 226 (2020), 117636, https://doi.org/10.1016/j.saa.2019.117636.
[17] M.R. Alcaráz, A. Schwaighofer, H. Goicoechea, B. Lendl, EC-QCL mid-IR transmission spectroscopy for monitoring dynamic changes of protein secondary structure in aqueous solution on the example of β-aggregation in alcohol-denaturated α-chymotrypsin, Anal. Bioanal. Chem. 408 (2016) 3933–3941, https://doi.org/10.1007/s00216-016-9464-5.
[18] A. Schwaighofer, M.R. Alcaráz, C. Araman, H. Goicoechea, B. Lendl, External cavity-quantum cascade laser infrared spectroscopy for secondary structure analysis of proteins at low concentrations, Sci. Rep. 6 (2016) 1–10, https://doi.org/10.1038/srep33556.
[19] A. Dabrowska, A. Schwaighofer, S. Lindner, B. Lendl, Mid-IR refractive index sensor for detecting proteins employing an external cavity quantum cascade laser-based Mach-Zehnder interferometer, Opt. Express 28 (2020) 36632–36642, https://doi.org/10.1364/oe.403981.
[20] S. Lindner, J. Hayden, A. Schwaighofer, T. Wolflehner, C. Kristament, M. González-Cabrera, S. Zlabinger, B. Lendl, External cavity quantum cascade laser-based mid-infrared dispersion spectroscopy for qualitative and quantitative analysis of liquid-phase samples, Appl. Spectrosc. 74 (2020) 452–459, https://doi.org/10.1177/0003702819892646.
[21] B. Stuart, Infrared Spectroscopy: Fundamentals And Applications, John Wiley & Sons, Ltd, 2004.
[22] A. Schwaighofer, M. Montemurro, S. Freitag, C. Kristament, M.J. Culzoni, B. Lendl, Beyond fourier transform infrared spectroscopy: external cavity quantum cascade laser-based mid-infrared transmission spectroscopy of proteins in the amide I and

amide II region, Anal. Chem. 90 (2018) 7072–7079, https://doi.org/10.1021/acs.analchem.8b01632.
[23] D. Hofstetter, M. Beck, J. Faist, Quantum-cascade-Laser Struct. Photo (2002), https://doi.org/10.1063/1.1512954.
[24] F.R. Giorgetta, E. Baumann, M. Graf, Q. Yang, C. Manz, K. Köhler, H.E. Beere, D. A. Ritchie, E. Linfield, A.G. Davies, Y. Fedoryshyn, H. Jäckel, M. Fischer, J. Faist, D. Hofstetter, Quantum cascade detectors, IEEE J. Quantum Electron 45 (2009) 1039–1052, https://doi.org/10.1109/JQE.2009.2017929.
[25] J. Hillbrand, M. Krüger, S. Dal Cin, H. Knötig, J. Heidrich, A.M. Andrews, G. Strasser, U. Keller, B. Schwarz, High-speed quantum cascade detector characterized with a mid-infrared femtosecond oscillator, Opt. Express 29 (2021) 5774–5781, https://doi.org/10.1364/OE.417976.
[26] D. Hofstetter, M. Graf, T. Aellen, J. Faist, L. Hvozdara, S. Blaser, 23 GHz operation of a room temperature photovoltaic quantum cascade detector at 5.35 μm, Appl. Phys. Lett. 89 (2006), 061119, https://doi.org/10.1063/1.2269408.
[27] L. Gendron, M. Carras, A. Huynh, V. Ortiz, C. Koeniguer, V. Berger, Quantum cascade photodetector, Appl. Phys. Lett. 85 (2004) 2824–2826, https://doi.org/10.1063/1.1781731.
[28] R. Szedlak, A. Harrer, M. Holzbauer, B. Schwarz, J.P. Waclawek, D. Macfarland, T. Zederbauer, H. Detz, A.M. Andrews, W. Schrenk, B. Lendl, G. Strasser, Remote sensing with commutable monolithic laser and detector, ACS Photonics 3 (2016) 1794–1798, https://doi.org/10.1021/acsphotonics.6b00603.
[29] P. Jouy, M. Mangold, B. Tuzson, L. Emmenegger, Y.C. Chang, L. Hvozdara, H. P. Herzig, P. Wägli, A. Homsy, N.F. de Rooij, A. Wirthmueller, D. Hofstetter, H. Looser, J. Faist, Mid-infrared spectroscopy for gases and liquids based on quantum cascade technologies, Analyst 139 (2014) 2039–2046, https://doi.org/10.1039/c3an01462b.
[30] B. Schwarz, P. Reininger, H. Detz, T. Zederbauer, A.M. Andrews, W. Schrenk, G. Strasser, Monolithically integrated mid-infrared quantum cascade laser and detector, Sensors 13 (2013) 2196–2205, https://doi.org/10.3390/s130202196.
[31] B. Schwarz, P. Reininger, D. Ristanić, H. Detz, A.M. Andrews, W. Schrenk, G. Strasser, Monolithically integrated mid-infrared lab-on-a-chip using plasmonics and quantum cascade structures, Nat. Commun. 5 (2014) 1–7, https://doi.org/10.1038/ncomms5085.
[32] D. Hofstetter, J. Di, F.L. Hvozdara, H.-P. Herzig, ·M. Beck, CO_2 Isotope Sensor Using A Broadband Infrared Source, A Spectrally Narrow 4.4 μm Quantum Cascade Detector, And A Fourier Spectrometer, in: Appl. Phys. B, 103, 2011, pp. 967–970, https://doi.org/10.1007/s00340-011-4532-1.
[33] D. Hofstetter, F.R. Giorgetta, E. Baumann, Q. Yang, C. Manz, K. Köhler, Midinfrared quantum cascade detector with a spectrally broad response, Appl. Phys. Lett. 93 (2008), 221106, https://doi.org/10.1063/1.3036897.
[34] A. Harrer, Quantum cascade intersubband devices for mid-infrared sensing, Wien (2017). ⟨http://www.ub.tuwien.ac.athttp//www.ub.tuwien.ac.at/eng⟩. accessed March 24, 2021.
[35] A. Wittmann, T. Gresch, E. Gini, L. Hvozdara, N. Hoyler, M. Giovannini, J. Faist, High-performance bound-to-continuum quantum-cascade lasers for broad-gain applications, IEEE J. Quantum Electron. 44 (2008) 36–40, https://doi.org/10.1109/JQE.2007.909516.
[36] A. Jollivet, B. Hinkov, S. Pirotta, H. Hoang, S. Derelle, J. Jaeck, M. Tchernycheva, R. Colombelli, A. Bousseksou, M. Hugues, Short infrared wavelength quantum cascade detectors based on m-plane ZnO/ZnMgO quantum wells, Appl. Phys. Lett. 113 (2018), 251104, https://doi.org/10.1063/1.5058120ï.
[37] L. Butschek, S. Hugger, J. Jarvis, Microoptoelectromechanical systems-based external cavity quantum cascade lasers for real-time spectroscopy, Opt. Eng. 57 (2017) 1, https://doi.org/10.1117/1.OE.57.1.011010.
[38] H.L. Monaco, G. Zanotti, P. Spadon, M. Bolognesi, L. Sawyer, E.E. Eliopoulos, Crystal structure of the trigonal form of bovine beta-lactoglobulin and of its complex with retinol at 2.5 Å resolution, J. Mol. Biol. 197 (1987) 695–706, https://doi.org/10.1016/0022-2836(87)90476-1.
[39] S.J. Prestrelski, D.M. Byler, M.P. Thompson, D.M. Byler, M.P. Thompson, Effect of metal ion binding on the secondary structure of bovine α-lactalbumin as examined by infrared spectroscopy, Biochemistry 30 (1991) 8797–8804, https://doi.org/10.1021/bi00100a010.
[40] E.L. Malin, M.H. Alaimo, E.M. Brown, J.M. Aramini, M.W. Germann, H.M. Farrel, P.L.H. Mcsweeney, P.F. Fox, Solution Structures of Casein Peptides: NMR, FTIR, CD, and Molecular Modeling Studies of S1-Casein, 1–23, 2001. ⟨https://www.researchgate.net/publication/222109152⟩ (accessed April 9, 2021).
[41] D.M. Curley, T.F. Kumosinski, J.J. Unruh, H.M. Farrell, Changes in the secondary structure of bovine casein by fourier transform infrared spectroscopy: effects of calcium and temperature 1 (1998), https://doi.org/10.3168/jds.S0022-0302(98)75881-3.
[42] M.J. Culzoni, H.C. Goicoechea, G.A. Ibañez, V.A. Lozano, N.R. Marsili, A. C. Olivieri, A.P. Pagani, Second-order advantage from kinetic-spectroscopic data matrices in the presence of extreme spectral overlapping. A multivariate curve resolution-Alternating least-squares approach, Anal. Chim. Acta 614 (2008) 46–57, https://doi.org/10.1016/j.aca.2008.03.013.
[43] H. Bruus, Theoretical microfluidics, first, Oxford University Press Inc., 2008.
[44] S. Großhans, M. Rüdt, A. Sanden, N. Brestrich, J. Morgenstern, S. Heissler, J. Hubbuch, In-line Fourier-transform infrared spectroscopy as a versatile process analytical technology for preparative protein chromatography, J. Chromatogr. A. 1547 (2018) 37–44, https://doi.org/10.1016/j.chroma.2018.03.005.
[45] A. Schwaighofer, M.R. Alcaraz, L. Lux, B. Lendl, pH titration of β-lactoglobulin monitored by laser-based Mid-IR transmission spectroscopy coupled to chemometric analysis, Spectrochim. Acta - Part A Mol. Biomol. Spectrosc. 226 (2020), 117636, https://doi.org/10.1016/j.saa.2019.117636.
[46] F. Dousseau, M. Pézolet, Determination of the secondary structure content of proteins in aqueous solutions from their amide i and amide ii infrared bands. comparison between classical and partial least-squares methods, Biochemistry 29 (1990) 8771–8779, https://doi.org/10.1021/bi00489a038.
[47] M. Farrés, S. Platikanov, S. Tsakovski, R. Tauler, Comparison of the variable importance in projection (VIP) and of the selectivity ratio (SR) methods for variable selection and interpretation, J. Chemom. 29 (2015) 528–536, https://doi.org/10.1002/cem.2736.
[48] C.K. Akhgar, V. Nürnberger, M. Nadvornik, M. Velik, A. Schwaighofer, E. Rosenberg, B. Lendl, Fatty acid prediction in bovine milk by attenuated total reflection infrared spectroscopy after solvent-free lipid separation, Foods 10 (2021) 1054, https://doi.org/10.3390/foods10051054.

Alicja Dabrowska received her BSc degree (2013) from Wroclaw University of Science and Technology and MSc degree (2017) from the University of Applied Sciences Technikum Wien in Biomedical Engineering Sciences. Currently, she is a PhD student at the Institute of Chemical Technologies and Analytics, Technische Universität Wien, Austria. Under supervision of Prof. Bernhard Lendl she works on the development of novel interferometric QCL-based sensing schemes for broadband refractive index sensing of liquids and towards fully-integrated, on chip protein sensors.

Mauro David obtained his BSc degree (2017) in Electronic Engineering at the Politecnico di Milano and his MSc degree (2019) at the University of Applied Sciences Technikum Wien in Biomedical Engineering. Currently, he is a PhD student at the Institute of Solid State Electronics, Technische Universität Wien, Austria. His research focuses on surface plasmon photonics and mid-infrared on-chip sensors under supervision the of Prof. Gottfried Strasser.

Stephan Freitag holds a MSc in biotechnology from the University of Applied Sciences in Tulln. During his master thesis he focused on quantum cascade laser based infrared spectroscopy of proteins in aqueous solutions. Recently, he finished his PhD in the Lendl group, where he developed instrumentation and methods combining ultrasound particle manipulation and attenuated total reflection infrared spectroscopy for bacteria detection in water.

Aaron Maxwell Andrews received his Ph.D. in Materials from the University of California, Santa Barbara, USA in 2003. His research focuses on intersubband devices for the MIR and THz spectral range (including QCLs, QCDs, QCLDs, QWIPs, ICLs, and RTDs), optoelectronic nanostructures, materials growth and characterization with an emphasis on molecular beam epitaxy of semiconductor materials and metals on semiconductors. Since 2020, he is an Associate Professor at the Institute for Solid State Electronics, Technische Universität Wien, Austria, where he leads the epitaxy laboratory.

Gottfried Strasser received his Ph.D. degree in Physics from the University of Innsbruck, Austria, in 1991. In 2007 G. Strasser became full professor at the State University of New York in Buffalo and in 2009 at the TU Wien, Vienna, Austria, where he is heading the Institute of Solid State Electronics and directing the Center for Micro- and Nanostructures. He has 25 years of experience in the field of nano-science and -technology, and is heading a group developing optoelectronic materials and nanostructures. He was speaker of an FWF SFB project and a project from the Austrian Nanoinitiative and is member of various scientific advisory boards. G. Strasser authored more than 450 journal papers, 300 conference papers, and 1400 conference contributions in the related areas.

Borislav Hinkov received his Ph.D. degree in Physics from ETH Zürich, Switzerland, in 2015 in the group of Jérôme Faist. He then joined the group of Gottfried Strasser at TU Wien in 2016 as postdoctoral and currently senior postdoctoral researcher. B. Hinkov has more than 10 years of experience in the fields of micro-/nano-science and technology and established at TU Wien a group on new mid-IR materials and optoelectronic devices as well as novel mid-IR plasmonics and liquid and gas spectroscopy techniques. His current research focus lies on the development of novel monolithic mid-IR plasmonic-based lab-on-a-chip sensors for protein analysis and telecommunication applications, as well as optoelectronic devices based on exotic semiconductors like ZnO.

Andreas Schwaighofer is a postdoctoral researcher at the Institute of Chemical Technology and Analytics at TU Wien, Austria. His work focuses on applying spectroscopic methods to study the stability and structural changes of proteins upon external perturbation, ligand binding and denaturation. Currently, his research interests include QCL-IR transmission spectroscopy for protein analysis and application of laser-based IR spectroscopy for process monitoring.

Bernhard Lendl received his PhD degree in Technical Chemistry from Technische Universität Wien (TU Wien) in 1996. His research focuses on advancing analytical sciences through the development of novel analytical techniques and instrumentation based on infrared and Raman spectroscopy and their application to environmental and process analytical chemistry, material characterization as well as bio-medical diagnostics. In 2008, he co-founded the TU Wien spin-off company QuantaRed Technologies GmbH, which develops mid-IR laser based analyzers for liquids. Since 2011, he heads the research division on environmental and process analytical chemistry at TU Wien where he was appointed full professor for Vibrational Spectroscopy in 2016.